Pronounced Non-Condon Effect as the Origin of the Quantum Beat Observed in the Time-Resolved Absorption Signal from Excited-State *cis*-Stilbene

Kunihiko Ishii, Satoshi Takeuchi, and Tahei Tahara*

Molecular Spectroscopy Laboratory, RIKEN (The Institute of Physical and Chemical Research), 2-1 Hirosawa, Wako 351-0198, Japan

Received: September 14, 2007; In Final Form: November 28, 2007

We carried out wavelength-dispersed time-resolved absorption measurements of *cis*-stilbene to investigate the mechanism of the appearance of the ∼220 cm^{-1} oscillation, which has been assigned to the nuclear wavepacket motion of the S_1 state. The observed oscillatory pattern showed almost same amplitude and phase across the absorption peak at 645 nm, which indicates that the modulation of the transition intensity gives rise to the quantum beat. We also carried out a semiquantitative numerical simulation of the time-resolved absorption spectra based on the effective linear response theory, in which we newly incorporated the Herzberg−Teller coupling model by introducing a coordinate-dependence of the transition moment. The results of these experiments and simulation clearly showed that the intensity of the quantum beat arises from a significant coordinate dependence of the S_n←S_1 transition moment, i.e., non-Condon effect. It was concluded that the vibronic coupling of the S_n state with other electronic states is so large that the Herzberg−Teller coupling predominantly contributes to the intensity of the quantum beat of the totally symmetric ∼220 cm^{-1} vibration. The present work suggests a general importance of the non-Condon effect in spectroscopy involving highly excited electronic states.

1. Introduction

Tunable ultrashort light pulses on the order of 10 fs are now available thanks to the advance of laser technologies, which makes time-domain vibrational spectroscopy feasible to polyatomic molecules in solution. Time-domain vibrational spectroscopy is often referred as "observation of nuclear wavepacket motion", because an ultrashort pulse having duration shorter than a vibrational period can trace a real-time motion of nuclei of the molecule through the time-evolution of vibrationally coherent states. Real-time observation of nuclear wavepacket motion (or vibrational coherence) is a common issue of spectroscopy using ultrashort optical pulses, and the nuclear wavepacket motion has been observed in a variety of femtosecond time-resolved spectroscopies. Although the information obtained from time-domain vibrational measurements are equivalent to the frequency domain data in principle, the ultrafast time-domain measurement is advantageous for the study of short-lived transient species[1,2] as well as for observation of low-frequency vibrations in the terahertz region.[3−5] Especially, time-domain vibrational measurements are important to investigate nuclear wavepacket motion of excited states that undergo ultrafast chemical reactions, because they enable us to examine the relation between the initial nuclear motion and reaction coordinate of the molecules.[1,2,6−8] This kind of approach can shed new light on our understanding about realistic reaction coordinates of polyatomic molecules.[8]

Previously, we investigated ultrafast photoisomerization of the S_1 state of *cis*-stilbene, which is one of the most prototypical ultrafast photochemical reactions in solution, using time-resolved absorption spectroscopy with 40 fs time resolution.[1] We measured a rapid decay of the S_n←S_1 transient absorption and observed a clear oscillation that manifested a ∼220 cm^{-1} nuclear wavepacket motion of the S_1 state. The damping time of the wavepacket motion was much shorter (∼200 fs) than the ordinary vibrational dephasing time in solution (∼ a few picoseconds), which indicated a highly anharmonic nature of the reactive S_1 potential energy surface of *cis*-stilbene. Because the oscillation was damped much faster than the isomerization reaction, it was concluded that the observed nuclear wavepacket motion was not directly correlated with the isomerization coordinate. The observed vibration was considered "perpendicular" to the reaction coordinate.[1,8]

The frequency of the nuclear wavepacket motion observed in the ultrafast transient absorption measurement agreed very well with the frequency of the most prominent band (229 cm^{-1}) in the resonance Raman spectra of S_1 *cis*-stilbene reported by Matousek et al.[9,10] This vibration was assigned to a totally symmetric vibration that consists of C═C torsion, C-phenyl torsion and C-phenyl in-plane bending motions.[10,11] A corresponding oscillation was also observed in a femtosecond time-resolved photoionization study in the gas phase by Fuss et al.[12] Thus, among all vibrational modes of S_1 *cis*-stilbene, this ∼220 cm^{-1} mode appeared with the highest intensity in all the reported spectroscopic experiments. Therefore, it is desirable to clarify the situation that makes the ∼220 cm^{-1} mode carry significant intensity in these spectroscopic experiments. Especially, it is important to have a unified view for the results of transient absorption and resonance Raman experiments, because the mechanism of a nuclear wavepacket motion to gain the intensity in transient absorption is closely related to the mechanism for the same motion to appear in resonance Raman.[13] The correct understanding on the optical process and mechanism of the signal appearance is indispensable to adequately derive information about the excited-state properties through the observation of nuclear wavepacket motion.

* Author to whom correspondence should be addressed. Phone: +81-48-467-4592. Fax: +81-48-467-4539. E-mail: tahei@riken.jp.

10.1021/jp077402e CCC: $40.75
Published on Web 02/15/2008

To consider this problem, the wavelength-dispersion measurement of the time-resolved absorption is informative. Generally speaking, the intensity of oscillation observed in time-resolved absorption signals reflects a temporal modulation of the property of the relevant electronic transition that is associated with the nuclear wavepacket motion. The temporal spectral change of the transient absorption provides crucial information about the mechanism of the modulation induced by the nuclear wavepacket motion. Thanks to the intrinsic broad bandwidth of ultrashort light pulses, we can observe the essential part of the spectral change just by dispersing the probe pulse in the case of measurements using ultrashort pulse in the order of 10 fs. In addition, to understand the relevant optical process (semi-)quantitatively, theoretical consideration on the spectrally dispersed time-resolved absorption data is important. Kumar et al. recently reported a numerical method[14,15] based on the effective linear response theory[16−20] to simulate a spectral change induced by a nuclear wavepacket motion. Their approach greatly simplified the calculation of optical response (pump−probe signal) and provided a practical way to simulate the pump−probe signals observed for real molecular systems. This method was applied to a heme protein, and the amplitude and phase profiles of coherent oscillations were successfully reproduced for both of electric-field-driven and reaction-driven coherences.[14] This approach has been used also for other systems to obtain a physical insight from the observed pump−probe signals.[21,22] Although the optical process of femtosecond time-resolved absorption spectroscopy can be treated more generally in the framework of the third-order nonlinear optical process using density matrix formalism,[23] the approach based on the linear response theory provides a more intuitive picture.

In this paper, we report wavelength-dispersed time-resolved transient absorption measurements of S_1 *cis*-stilbene in a nonpolar solvent as well as numerical simulation based on the linear response theory. We extend the original formalism of Kumar et al. to include the non-Condon effect (coordinate dependence of the transition moment) to reproduce the wavelength-dispersed time-resolved absorption data of *cis*-stilbene. Based on the results of the experiment and simulation, we discuss the mechanism for the S_1 wavepacket motion to appear in the ultrafast transient absorption.

2. Methods

2.1. Experimental Procedure. Time-resolved absorption measurements were performed by an apparatus based on two laboratory-made noncollinear optical parametric amplifiers (NOPAs).[2,7] The output of a Ti:sapphire regenerative amplifier (Clark-MXR CPA-1000, 1 kHz, 1 mJ, ∼100 fs) was split into two (1:5) and used for pumping two NOPA units: one was a single-path NOPA to generate the probe pulse at ∼645 or ∼660 nm, and the other was a double-path NOPA that creates ultrashort pulses at ∼630 nm. The output of the second NOPA was frequency-doubled by a BBO crystal (50 μm) to generate an ultraviolet pulse (∼315 nm) that was used as the pump pulse. The pump and probe pulses were focused onto the same spot at the sample solution that formed a thin film-like jet with ∼50 μm thickness. In the wavelength-integrated measurements which we have already reported,[1] the probe pulse (∼660 nm) transmitted through the sample solution was detected by a photodiode (Hamamatsu S2281), and the absorption change induced by pump irradiation was measured.

In the wavelength-dispersed measurement, the probe pulse (∼645 nm) that passed through the sample was collected by a fiber bundle and then introduced into a spectrograph (Chromex 500is/sm, 150 gr/mm grating) equipped with a CCD camera (Princeton instruments TEA/CCD-1024-EM/1 UV). The probe spectrum before the sample was also measured in the same way, and it was used as the reference spectrum. The output of the Ti:sapphire regenerative amplifier was chopped by a synchronous chopper (New Focus 3501) at 100 Hz, and 5 shots were accumulated in each single exposure of the CCD camera. The pump pulse was additionally modulated by another synchronous chopper at 50 Hz, and the probe spectrum with and without pump was collected alternately to minimize the effect of slow fluctuation of the laser pulses. Obtained probe spectra were divided by reference spectra to compensate small spectral fluctuation of the probe pulse, and the pump-induced absorption change was calculated from two corrected probe spectra measured with and without the pump pulse. The cross-correlation between the pump and probe pulses was measured by difference frequency generation (DFG) with use of a thin BBO crystal (50 μm) and a photodiode, and the time resolution of the measurements was evaluated to be 40−50 fs (fwhm of the cross correlation). In all measurements, the polarization angle between the pump and probe pulses was set at the magic angle.

cis-Stilbene was purchased from Aldrich, and it was used as received. Because a noticeable amount (∼0.3%) of *trans*-isomer was contained in the purchased sample, we had to subtract its contribution from the observed data. We separately measured time-resolved spectra of the *trans*-isomer and subtracted them from *cis*-stilbene data by matching the transient absorption intensity at 10 ps where *cis*-isomer does not contribute. Spectroscopic grade cyclohexane was obtained from Wako Pure Chemical and was used without further purification.

2.2. Theoretical Analysis. For theoretical analysis, we extended the effective linear response approach of Kumar et al. to include the non-Condon effect. In the following, we describe the framework of the effective linear response approach as well as our extension.

The optical process of ultrafast pump−probe spectroscopy is generally represented as a third-order nonlinear optical process. Thus, the simulation of the wavelength-dispersed pump−probe signal requires an evaluation of the relevant third-order nonlinear susceptibility $\chi^{(3)}(\omega;\ \omega_{\mathrm{pump}},\omega_{\mathrm{pump}},\omega_{\mathrm{probe}})$ that simultaneously incorporates both pump and probe processes.[23] In the effective linear response approach, however, the pump and probe processes are treated separately, which can provide a more intuitive picture. The probe process is treated as a quasi-stationary linear response of the vibrationally coherent electronic excited state (S_1 *cis*-stilbene in this work) that is prepared by the pump process. Therefore, the quantum beat of the pump−probe signal is considered through a temporal modulation on the quasi-stationary linear response of the S_1 state (Figure 1a). This treatment is relevant only when the pump and probe pulses are practically separated in time (the well-separated pulse limit), but it is actually the time region of interest in most of studies.

In the effective linear response theory, the coherent state generated by the pump pulse is represented by a nonstationary nuclear wavepacket on the photoexcited electronic state. The motion of this nuclear wavepacket is modeled, in the first-order approximation, by the motion of the thermally equilibrated nuclear wavepacket along the relevant coordinate, with keeping its original shape (i.e., the change in the second and higher order moments is neglected).[14] This modeling is theoretically formulated using the following displacement operator $\hat{D}(\lambda)$,

$$\delta\hat{\rho} = \hat{D}(\lambda)\,\hat{\rho}_{\mathrm{T}}\hat{D}^{\dagger}(\lambda) \tag{1}$$

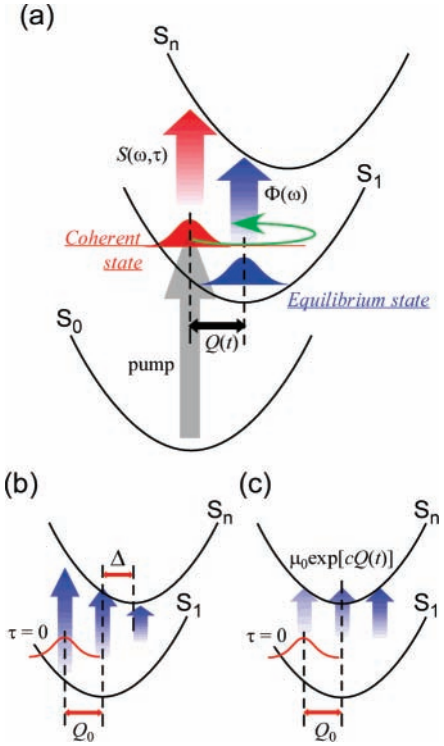

Figure 1. Two types of potential energy surfaces considered in the numerical simulation. (a) Schematic illustration for the effective linear response approach. Relations between the S_1 and S_n potentials relevant to the probe process for (b) the Franck−Condon model and (c) the Herzberg−Teller model.

where $\hat{\rho}_T$ is the density matrix of the excited-state in the thermal equilibrium and $\delta\hat{\rho}$ is that of the vibrationally coherent state. λ represents displacements of the first moment in the coordinate (Q_0) and momentum (P_0) space,

$$\lambda = \frac{Q_0 + iP_0}{\sqrt{2}} \tag{2}$$

In order to simulate actual pump−probe signals, we consider a time-resolved pump−probe experiment with a probe pulse having a center frequency ω_c and the pump−probe delay set at τ. The pump−probe signal $S(\tau)$ is expressed by using the envelope of the probe field $E(t)$ and that of the polarization of material $P(t,\tau)$:

$$S(\tau) = -\frac{\omega_c}{2} \mathrm{Im} \int_{-\infty}^{\infty} dt\, E^*(t-\tau)\, P(t,\tau) = \int_0^{\infty} \tilde{S}(\omega,\tau)\, d\omega \tag{3}$$

Here, $\tilde{S}(\omega,\tau)$ is a wavelength-dispersed signal at frequency ω. This $\tilde{S}(\omega,\tau)$ can be represented as follows, within the rotating wave approximation:

$$\tilde{S}(\omega,\tau) = -\frac{\omega}{4\pi} \mathrm{Im}\{e^{-i(\omega-\omega_c)\tau} \tilde{E}^*(\omega-\omega_c)\, \tilde{P}(\omega-\omega_c,\tau)\} \tag{4}$$

where $\tilde{E}(\omega)$ and $\tilde{P}(\omega,\tau)$ denote the Fourier transform of $E(t)$ and $P(t,\tau)$, respectively. The polarization $P(t,\tau)$ is derived from the effective linear response $\chi^{\mathrm{eff}}(t,t_0)$:

$$P(t,\tau) = \int_0^{\infty} ds\, e^{i\omega_c s} \chi^{\mathrm{eff}}(t,t-s)\, E(t-s-\tau) \tag{5}$$

The effective linear response $\chi^{\mathrm{eff}}(t,t_0)$ is, in turn, related to $\delta\hat{\rho}$ and the electric dipole moment operator $\hat{\mu}(t)$ as

$$\chi^{\mathrm{eff}}(t,t_0) = \frac{i}{\hbar} \mathrm{Tr}(\hat{\mu}(t)[\hat{\mu}(t_0),\delta\hat{\rho}]) \tag{6}$$

Here, we assume that only two electronic states are involved in the probe process, which are the S_1 and S_n states in the present case. Then, using the transition moment $\hat{\mu}_0$ and the transition frequency ω_0 between these two states, we can calculate $\chi^{\mathrm{eff}}(t,t_0)$ as

$$\chi^{\mathrm{eff}}(t,t_0) = \frac{i}{\hbar} e^{-i\omega_0(t-t_0)} \mathrm{Tr}\left[\delta\hat{\rho}\, \hat{\mu}_0(t) \exp\left(-\frac{i}{\hbar}\int_{t_0}^{t} ds\, \hat{V}(s)\right)_+ \hat{\mu}^*_0(t_0)\right] + \mathrm{c.c.} \tag{7}$$

where $\hat{V}(s)$ denotes the time-dependent part of the energy difference between the two electronic states, and c.c. denotes the complex conjugate. The plus sign of the exponential function indicates that it is the time-ordered exponential function.[23]

To derive the formula that will be used for actual numerical simulations, we consider two types of the electron−nuclear coupling, i.e., Franck−Condon coupling and Herzberg−Teller coupling, as described below.

2.2.1. Franck−Condon Coupling. In the original work of Kumar et al., they employed the Condon approximation and neglected nuclear-coordinate dependence of the transition dipole, i.e., $\hat{\mu}_0(t) = \mu_0$. In addition, they assumed a pair of harmonic potentials with displacement Δ and a common harmonic frequency ω_f for the S_1 and S_n states that are involved in the probe process (Figure 1b). Within this approximation, the band shape of the electronic transition is solely determined by the Franck−Condon factor, so that we call this type of electron−nuclear coupling "Franck−Condon coupling", hereafter. In this case, the representation of $\chi^{\mathrm{eff}}(t,t_0)$ is simplified as

$$\chi^{\mathrm{eff}}(t,t_0) = \frac{i}{\hbar}|\mu_0|^2 e^{-i\omega_0(t-t_0)} \mathrm{Tr}\left[\delta\hat{\rho} \exp\left(-\frac{i}{\hbar}\int_{t_0}^{t} ds\, \hat{V}(s)\right)_+\right] + \mathrm{c.c.} \tag{8}$$

Then, because the energy difference between the two electronic states is a linear function of the coordinate ($\hat{V} = -\hbar\omega_f\Delta\hat{Q}$), we obtain

$$\chi^{\mathrm{eff}}(t,t_0) = \frac{i}{\hbar}|\mu_0|^2 e^{-i\omega_0(t-t_0)} \mathrm{Tr}[\hat{\rho}_T \times \exp(i\omega_f\Delta \int_{t_0}^{t} ds\, \hat{D}^{\dagger}(\lambda)\, \hat{Q}(s)\, \hat{D}(\lambda))_+] + \mathrm{c.c.} \tag{9}$$

Here, the displacement operator $\hat{D}(\lambda)$ has the following property:

$$\hat{D}^{\dagger}(\lambda)\, \hat{Q}(s)\, \hat{D}(\lambda) = \hat{Q}(s) + \bar{Q}(s) \tag{10}$$

$$\bar{Q}(s) = \sqrt{2}\, \mathrm{Re}\{\lambda\, e^{-i\omega_f s}\} \tag{11}$$

Using this relation (10), we can factor out from eq 9 a correlation function $K(t-t_0)$ that represents the absorption spectrum of the S_1 state in thermal equilibrium. By describing the coherent nuclear motion of the S_1 state as $\bar{Q}(s) = Q_0 \cos \omega_f s$ (which neglects damping and sets the initial momentum at $P_0 = 0$), we obtain

$$\chi^{\mathrm{eff}}(t,t_0) = \frac{i}{\hbar}|\mu_0|^2 K(t-t_0) \exp(i\, Q_0\Delta \sin \omega_f t) \times \exp(-i\, Q_0\Delta \sin \omega_f t_0) + \mathrm{c.c.} \tag{12}$$

Combining eq 12 with eqs 4 and 5 within the rotating wave approximation and collecting the first-order terms, we obtain the following formula that gives the oscillation in the wavelength-dispersed pump−probe signal.[14] (We omit the tilde in the notation hereafter.)

$$S(\omega,\tau) = -\frac{|\mu_0|^2}{4\pi\hbar}\omega E^*(\omega_d)\, J_1(Q_0\Delta)\, J_0(Q_0\Delta)(C_I \cos\omega_f\tau - C_R \sin\omega_f\tau) \quad (13)$$

$$C_I = E(\omega_d+\omega_f)\{\Phi_I(\omega+\omega_f)-\Phi_I(\omega)\} + E(\omega_d-\omega_f)\{\Phi_I(\omega)-\Phi_I(\omega-\omega_f)\}$$

$$C_R = E(\omega_d+\omega_f)\{\Phi_R(\omega+\omega_f)-\Phi_R(\omega)\} - E(\omega_d-\omega_f)\{\Phi_R(\omega)-\Phi_R(\omega-\omega_f)\}$$

where $\omega_d = \omega - \omega_c$. $J_m(x)$ is an mth order Bessel function, and $\Phi_{R,I}(\omega)$ are the real and imaginary parts of the complex line shape function $\Phi(\omega) = i\int_0^\infty ds\, e^{i\omega s} K(s)$.

2.2.2. Herzberg−Teller Coupling. In this work, we extended the theoretical treatment of Kumar et al. to incorporate the non-Condon effect. So far, there have already been a few reports on the simulation of pump−probe absorption signals which takes the non-Condon effect into account based on the third-order nonlinear polarization.[24,25] However, there is no established way to carry out a semiquantitative simulation focusing on a three-state system, which is applicable to our two-color pump−probe absorption experiment. We introduced the non-Condon effect to the effective linear response approach by assuming a coordinate-dependent transition moment in eq 7. This extension allows us to simulate a pump−probe absorption signal also in the non-Condon case, without losing the simplicity and physical clarity of the original method. Hereafter, in analogy with the Herzberg−Teller expansion to describe non-Condon effects in electronic transitions, we refer to this type of nuclear−electron coupling due to the non-Condon effect as "Herzberg−Teller coupling".

Assuming non-displaced harmonic potentials ($\hat{V}(s) = 0$) with an exponential coordinate dependence of the transition moment ($\hat{\mu}_0(t) = \mu_0 \exp[c\hat{Q}(t)]$,[24] $c \ll 1$, Figure 1c), the effective linear response given in eq 7 becomes

$$\begin{aligned}
\chi^{eff}(t,t_0) &= \frac{i}{\hbar} e^{-i\omega_0(t-t_0)}\, \mathrm{Tr}[\delta\hat{\rho}\,\mu_0\, e^{c\hat{Q}(t)}\,\mu_0^*\, e^{c\hat{Q}^*(t_0)}] + \text{c.c.} \\
&= \frac{i}{\hbar} e^{-i\omega_0(t-t_0)}\, \mathrm{Tr}[\hat{D}(\lambda)\,\hat{\rho}_T\hat{D}^\dagger(\lambda)\,\mu_0\, e^{c\hat{Q}(t)}\,\mu_0^*\, e^{c\hat{Q}^*(t_0)}] + \text{c.c.} \\
&= \frac{i}{\hbar} e^{-i\omega_0(t-t_0)}\, \mathrm{Tr}[\hat{\rho}_T\mu_0\, e^{c\hat{D}^\dagger(\lambda)\hat{Q}(t)\hat{D}(\lambda)}\,\mu_0^* e^{c\hat{D}^\dagger(\lambda)\hat{Q}^*(t_0)\hat{D}(\lambda)}] + \text{c.c.} \\
&= \frac{i}{\hbar} e^{-i\omega_0(t-t_0)}\, \mathrm{Tr}[\hat{\rho}_T\mu_0\, e^{c(\hat{Q}(t)+\bar{Q}(t))}\,\mu_0^*\, e^{c(\hat{Q}(t_0)+\bar{Q}(t_0))}] + \text{c.c.} \\
&= \frac{i}{\hbar}|\mu_0|^2 K(t-t_0)\, e^{c\bar{Q}(t)}\, e^{c\bar{Q}^*(t_0)} + \text{c.c.} \\
&\sim \frac{i}{\hbar}|\mu_0|^2 K(t-t_0)\{1 + cQ_0(\cos\omega_f t + \cos\omega_f t_0)\} + \text{c.c.} \quad (14)
\end{aligned}$$

Using this form of the effective nonlinear response, we obtain the following first-order oscillatory term of the wavelength-dispersed time-resolved absorption signal for the case of the Herzberg−Teller coupling:

$$S(\omega,\tau) = -\frac{|\mu_0|^2}{8\pi\hbar}\omega c Q_0 E^*(\omega_d)(C_I \cos\omega_f\tau + C_R \sin\omega_f\tau) \quad (15)$$

$$C_I = E(\omega_d+\omega_f)\{\Phi_I(\omega)+\Phi_I(\omega+\omega_f)\} + E(\omega_d-\omega_f)\{\Phi_I(\omega)+\Phi_I(\omega-\omega_f)\}$$

$$C_R = E(\omega_d+\omega_f)\{\Phi_R(\omega)+\Phi_R(\omega+\omega_f)\} - E(\omega_d-\omega_f)\{\Phi_R(\omega)+\Phi_R(\omega-\omega_f)\}$$

3. Results

3.1. Wavelength-Integrated Measurements. The results of wavelength-integrated measurements were already reported in the previous paper.[1] Thus, we only give a brief description of principal conclusions. A time-resolved absorption signal obtained from *cis*-stilbene in cyclohexane (5×10^{-2} mol dm^{-3}) is shown in Figure 2a. The $S_n \leftarrow S_1$ transient absorption decays within a few picoseconds, corresponding to the isomerization in the S_1 state. The signal clearly shows an oscillatory feature in the femtosecond region, which was assigned to the nuclear wavepacket motion (the vibrational coherence) in the S_1 state.[1] By subtracting population decay that was fitted by two exponential functions, an oscillating component is extracted in Figure 2b. The central frequency of the Fourier-transform of this oscillation is around 220 cm^{-1}. This frequency is in good agreement with the frequency of a spontaneous Raman band of S_1 *cis*-stilbene observed in the frequency domain ($\sim$229 cm^{-1}).[10] This vibrational mode was assigned to a totally symmetric vibration that consists of C=C torsion, C-phenyl torsion and C-phenyl in-plane bending motions by a vibrational analysis based on a CIS calculation.[10,11]

3.2. Wavelength-Dispersed Measurement. In the measurement described above,[1] the pump−probe absorption signal was measured by only monitoring the total intensity change of the probe pulse transmitted through the sample. In this study, we dispersed the probe pulse before detection and examined the delay-time dependent spectral change. This experiment provided information not only about the change of the transient absorption intensity but also about the spectral change accompanying the oscillation due to the 220 cm^{-1} wavepacket motion.

The spectrum of the probe pulse (before the sample) is shown in Figure 3. Since it covers a wavelength range around the intensity maximum of the $S_n \leftarrow S_1$ absorption of *cis*-stilbene, it can sensitively detect the most crucial part of the spectral change of the transient absorption. We note that the time resolution of the measurement was not deteriorated by the wavelength dispersion, because the probe pulse preserved its ultrashort pulse-width at the sample point, and the dispersion was carried out afterward. In other words, we can trace time-dependent spectral changes, maintaining the highest time resolution that can be obtained from the probe pulse.

Figure 4a shows a time-wavelength two-dimensional plot of the transient absorption signal of *cis*-stilbene in cyclohexane (5×10^{-2} mol dm^{-3}). The time profiles at the blue-side, peak, and red-side around the $S_n \leftarrow S_1$ absorption maximum are separately shown in Figure 4b. We recognized a very slight temporal shift of the time origin, depending on the wavelength. This shift is due to a residual chirp of the probe pulse, which was not fully compensated by a prism pair inserted in the probe beam path. The main feature of the time profile at each wavelength is almost identical to the wavelength-integrated data, i.e., a clear oscillation that dephases with a time constant of $\sim$200 fs on the population decay ($\tau \sim 1$ ps). The most notable feature in the wavelength-dispersed data is the invariance over the whole wavelength range observed. There is no phase flip

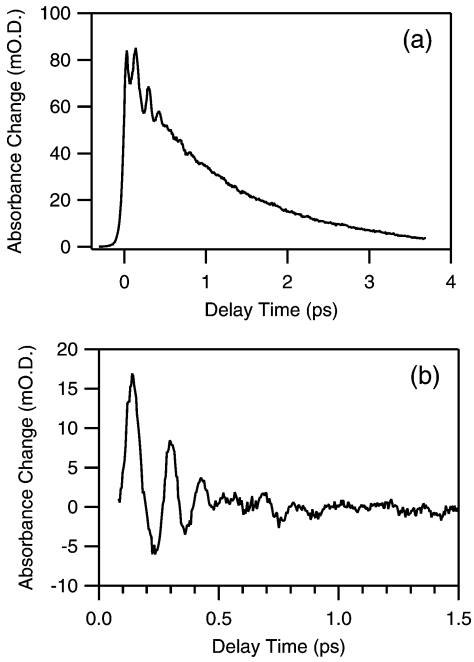

Figure 2. (a) Time-resolved absorption signal of *cis*-stilbene in cyclohexane (5×10^{-2} mol dm^{-3}).[1] The pump and probe wavelengths are 315 and 660 nm, respectively. (b) The oscillatory component extracted by subtraction of the population component.

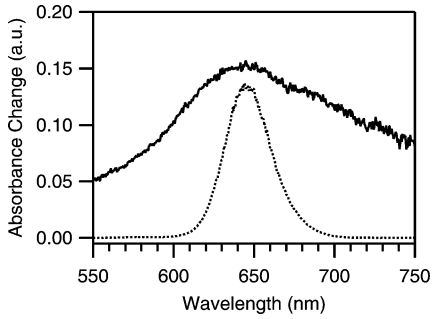

Figure 3. Time-resolved absorption spectrum of *cis*-stilbene in cyclohexane (5×10^{-3} mol dm^{-3}) measured at 0.5 ps after 267 nm excitation with subpicosecond time resolution (solid line).[1] The intensity spectrum of the probe pulse used in the wavelength-dispersed measurement is also shown (dotted line).

of the oscillation around the absorption peak, and the relative amplitudes of the oscillation are very similar at all wavelengths. This is in clear contrast to the ordinary spectral change induced by the nuclear wavepacket motion. In usual cases, the spectrum itself moves back and forth along the wavelength axis, keeping its integrated intensity. The oscillations show the π phase shift across the absorption maximum, and hence the oscillation disappears at the peak wavelength.[14] This type of usual oscillation has been reported for several typical systems.[26,27] In the present case of S_1 *cis*-stilbene, however, the transient absorption shows an oscillation that exhibits the same phase at every wavelength. In other words, the integrated intensity of the $S_n \leftarrow S_1$ absorption is modulated with the delay time, implying that the $S_n \leftarrow S_1$ transition intensity itself changes with time. It is clear that the origin of the observed oscillation is not a simple transition energy modulation. Actually, the origin is a transition intensity modulation.

We note that signal oscillation arising from the transition intensity modulation has already been reported for a few systems. Rubtsov and Yoshihara observed the wavepacket motion of charge-transfer complexes in the excited state by femtosecond fluorescence upconversion.[28] They found that the

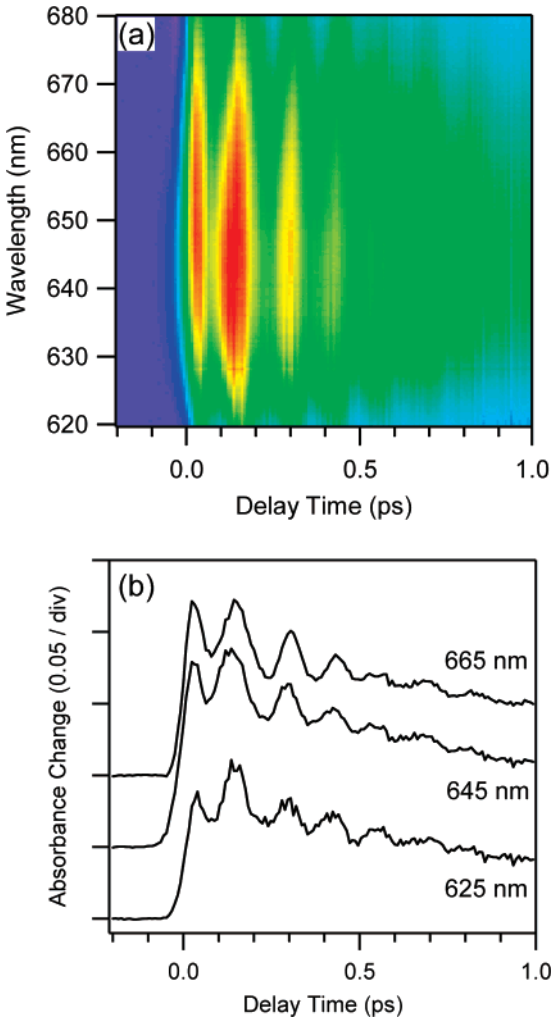

Figure 4. (a) Wavelength-dispersed time-resolved absorption signal of *cis*-stilbene in cyclohexane (5×10^{-2} mol dm^{-3}) with 315 nm pump. (b) Temporal profiles at 625, 645, and 665 nm. These wavelengths correspond to the blue side, peak, and red side of the $S_n \leftarrow S_1$ absorption band, respectively. The slight wavelength-dependent shift of the time origin is due to a residual chirp of the probe pulse.

coherent motion appears in the fluorescence signal through both of the transition frequency modulation and the transition intensity modulation. Kano et al. observed a nuclear wavepacket motion in porphyrin J-aggregates using sub-5 fs pump−probe absorption spectroscopy.[29] They analyzed the phase and amplitude of the oscillations observed in the wavelength-dispersed absorption spectra, and concluded that the oscillation arose from the transition intensity modulation that was induced by a "dynamic intensity borrowing" (which is actually vibronic coupling). In these studies, however, the transition intensity modulation was observed for the transition between the ground state and S_1 state. In this work, we observed the transition intensity modulation for the transition between the S_1 state and the highly excited upper state (S_n).

3.3. Numerical Simulation. To compare the experimental data with theoretical simulation, we carried out a numerical simulation based on the formalism described in section 2.2. In this simulation, we used the transient absorption spectrum of thermally equilibrated S_1 *cis*-stilbene and the probe pulse spectrum to determine $\Phi(\omega)$ and $E(\omega)$, respectively, in eq 13 and eq 15. Briefly, we fitted the transient absorption spectrum measured at 0.5 ps (Figure 3) with a sum of two Gaussian functions, and divided it by ω to obtain the imaginary part of the line shape function, $\Phi_I(\omega)$. Then, the real part, $\Phi_R(\omega)$, was

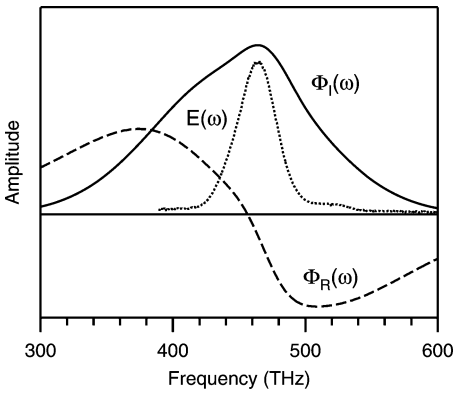

Figure 5. The line shape functions $\Phi_I(\omega)$ (solid line) and $\Phi_R(\omega)$ (dashed line) derived from an experimental transient absorption spectrum (Figure 2). Probe field spectrum $E(\omega)$ is also shown (dotted line).

calculated by the Hilbert transformation (Kramers−Kronig relations) from $\Phi_I(\omega)$. $E(\omega)$ was simply obtained as the square root of the intensity spectrum of the probe pulse. The obtained spectra of $\Phi_I(\omega)$, $\Phi_R(\omega)$ and $E(\omega)$ are shown in Figure 5. We neglected the phase structure (chirp) of the probe pulse in the simulation because it is not significant in the present experiment.

Figure 6 shows the results of the simulations for the two types of the electron−nuclear coupling, i.e., the Franck−Condon coupling and Herzberg−Teller coupling. In both cases, we assumed a single intramolecular vibrational mode at $\omega_f = 220$ cm^{-1}. The parameters that determine the amplitude of oscillation ($Q_0\Delta$ and cQ_0) were set at arbitrary values so that the simulation well reproduced the experimental data. Note that we did not take account of the dephasing process of nuclear wavepacket motion in this simulation. Consequently, deviations from the experimental data are seen in the long delay time region, owing to damping of the oscillatory signal in the experimental data. However, it is not the point of our discussion and hence does not affect our following arguments. The simulation for the Franck−Condon coupling (Figure 6a) gives an oscillatory pattern with a phase flip at the absorption peak around 645 nm, and the oscillation completely diminishes at the peak. In contrast, the simulation for the Herzberg−Teller coupling (Figure 6b) shows an absorption signal that oscillates in phase at every wavelength, and the relative amplitude of the oscillation is virtually wavelength independent. Clearly, the experimental data (Figure 6c) agree well with the case of the Herzberg−Teller coupling. It confirms that the origin of the observed oscillation of transient absorption is the modulation of the $S_n \leftarrow S_1$ transition intensity induced by the S_1 nuclear wavepacket motion having a frequency of $\sim$220 cm^{-1}.

4. Discussion

On the basis of the wavelength-dispersed time-resolved absorption data and the results of theoretical simulations, we can safely conclude that the oscillation of the $S_n \leftarrow S_1$ absorption signal of *cis*-stilbene arises from the transition intensity modulation that is induced by the 220 cm^{-1} wavepacket motion in the S_1 state. In other words, the Herzberg−Teller coupling due to the 220 cm^{-1} vibration induces a significant change in the $S_n \leftarrow S_1$ transition intensity, which makes the relevant wavepacket motion give rise to an oscillatory feature in the pump−probe signal.

Interestingly, this mechanism is different from the mechanism that has been claimed for the same S_1 vibration to appear in resonance Raman spectra.[9,10] In the picosecond Raman spectra of S_1 *cis*-stilbene that was in resonance with the same $S_n \leftarrow S_1$ absorption, the same vibration exhibited a prominent Raman band. Moreover, this S_1 vibration exhibited very strong progressions up to the second overtone, while no other fundamental vibrations showed noticeable bands in the Raman spectra. The appearance of the overtones in the resonance Raman spectra is an unambiguous evidence that the potential minimum of the S_1 state is significantly displaced from the S_n minimum along the corresponding coordinate. Because a significant potential displacement is a typical situation that makes strong resonance Raman signals appear by the Franck−Condon coupling, Kwok et al. argued that the Franck−Condon coupling (Albrecht's A term) is the mechanism for this vibration to gain a high resonance Raman intensity.[10] Their conclusion for resonance Raman data looks out of harmony with our conclusion for the pump−probe data, because a significant displacement between the two potentials and a significant vibronic coupling are not usually claimed simultaneously as the mechanism for a particular vibration to appear in spectroscopic data that are related to the same electronic transition. Actually, this apparent inconsistency seems to indicate a unique (but presumably more or less general) feature of the $S_n \leftarrow S_1$ transition, as discussed below.

In traditional molecular spectroscopy, the signal intensity and relevant mechanism are usually discussed on the basis of the following expansion of the transition moment:

$$\mu_{f\leftarrow i} = \langle f|\hat{\mu}|i\rangle\langle v_f|v_i\rangle + \sum_{e\neq f} \frac{\left\langle f\left|\left(\frac{\partial H}{\partial Q}\right)_{Q=0}\right|e\right\rangle}{\Delta E_{ef}} \langle e|\hat{\mu}|i\rangle\langle v_f|Q|v_i\rangle + \ldots \quad (16)$$

In this expansion, the first term represents the Franck−Condon coupling and the second denotes the Herzberg−Teller coupling. The first term is considered much larger than the second term when the f←i electronic transition is optically allowed. Thus, for totally symmetric vibrations, the first term is responsible for the vibrational transition that occurs along with the f←i electronic transition. It means that when there is a vibrational coordinate along which the potential minima of the i and f electronic states are displaced, the corresponding vibration exhibits a progression in the f←i absorption as well as f→i fluorescence, and also shows a strong vibrational bands in Raman spectra resonant with the f←i electronic transition. However, this first term does not contribute to the vibronic transition of non-totally symmetric vibrations, because the two potentials cannot be displaced along non-totally symmetric coordinates under harmonic approximation. Thus, the second term becomes the leading term for the vibronic transition of non-totally symmetric vibrations, and only $\Delta v = \pm 1$ transition appears in the spectra. Consequently, in the framework of traditional spectroscopy, the potential displacement and vibronic coupling are not considered simultaneously as the mechanism for a particular vibration to appear in the electronic spectra and resonance Raman spectra. Actually, this common sense is the reason of uneasiness that we feel from the apparent inconsistency between the mechanisms of the appearance of the oscillation in the pump−probe signal and the intense vibrational band in resonance Raman.

Here, we note that the above-described common sense is based on the assumption that the first term of the expansion in eq 16 is much larger than the second term for totally symmetric vibrations. This assumption is valid when we consider the transition from the S_0 state to the S_1 state (or that from the S_0

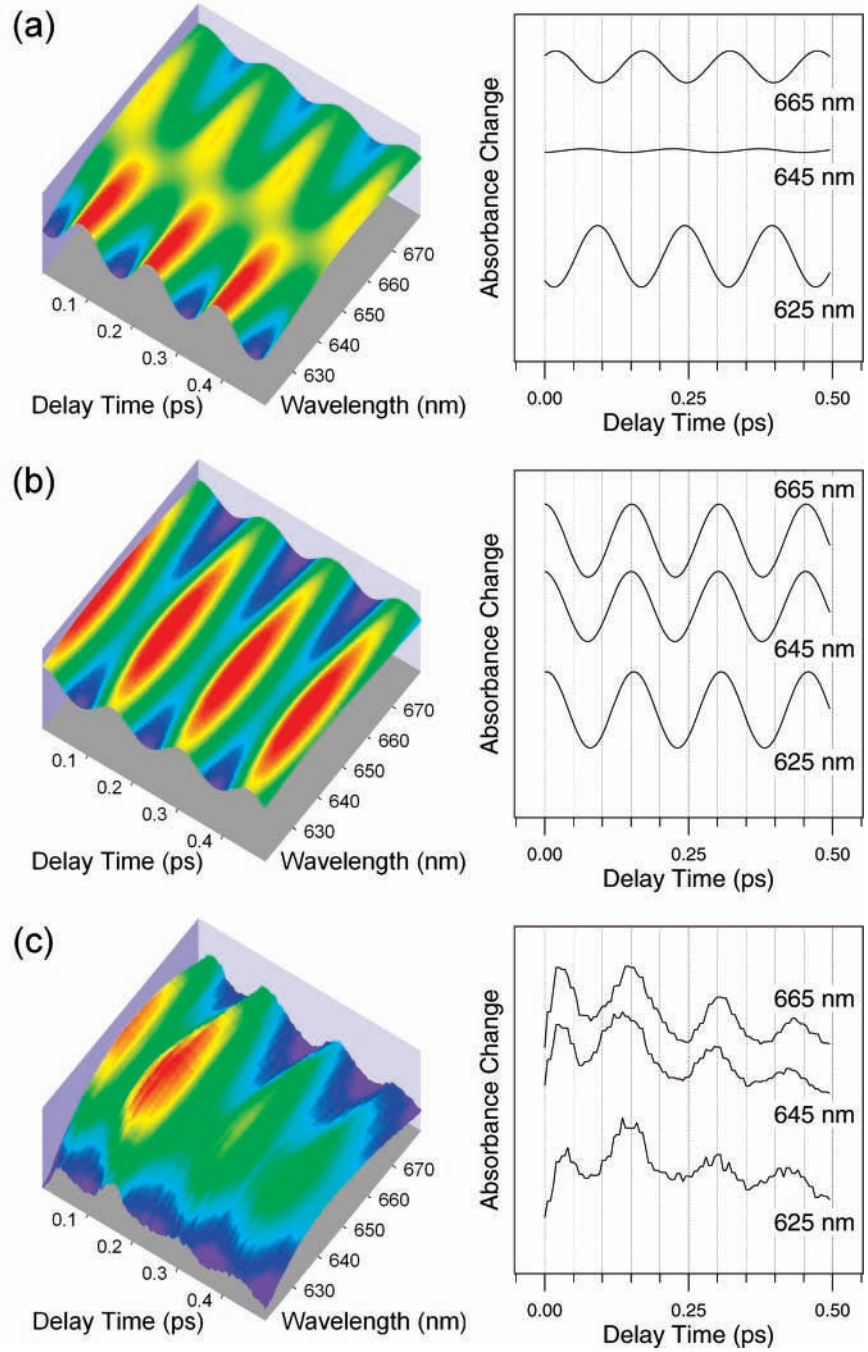

Figure 6. Results of numerical simulations based on the effective nonlinear response theory. (a) The Franck−Condon model and (b) the Herzberg−Teller model. The experimentally observed signal is shown in (c) for comparison. Panels at right are temporal profiles at 625, 645, and 665 nm of each two-dimensional plot.

state to a low-lying S_n state). However, for the transition from the S_1 state to highly excited S_n states, we think that it is not necessarily valid. In fact, the common sense in traditional spectroscopy has been formed mainly on the basis of the studies on the electronic transition from the S_0 state to very low-lying excited states, so that even the final excited state of the transition is well isolated in energy from other optically active excited states (i.e., ΔE_{ef} in eq 16 is fairly large). In contrast, the transient absorption measurement monitors the electronic transition from the S_1 state to a highly excited S_n state, and it is expected that a number of excited states are closely located around the S_n state in the high energy region. This situation of the S_n state results in much smaller ΔE_{ef}, which can make the magnitude of the second term of eq 16 comparable to, or even larger than, the first term. Therefore, the Herzberg−Teller coupling can be more responsible as the mechanism for totally symmetric vibrations to gain signal intensity in spectroscopy that is relevant to the $S_n \leftarrow S_1$ transition.

We consider this is the key to solve the apparent inconsistency between the mechanisms for the ~220 cm^{-1} vibration to give rise to the significant oscillation in the wavelength-dispersed pump−probe absorption and to exhibit prominent overtones in resonance Raman spectra. In these two experiments, we observe the vibrational signal through the transition involving the highly excited S_n state. The present study clearly demonstrates that the 220 cm^{-1} vibration appears in the pump−probe data through the Herzberg−Teller coupling mechanism. Therefore, it is natural to consider that the very large non-Condon effect (the

vibronic coupling through a vibration) also gives the significant intensity to the 220 cm^{-1} vibration in resonance Raman spectra. In other words, we consider that the Herzberg−Teller coupling should predominantly contribute also to the Raman intensity of the 220 cm^{-1} mode of S_1 *cis*-stilbene, and the contribution from the Franck−Condon mechanism to the resonance Raman intensity is relatively small.

For the overtones in the resonance Raman spectra, it is important to note that the appearance of the overtones only indicates the existence of a significant displacement between the S_1 and S_n potentials, but it does not directly imply that the Raman intensity arises from the Franck−Condon mechanism. Actually, Albrecht and co-workers reported a general theory of Raman intensities for a situation where both the potential displacement and the non-Condon effect are significant.[30] They showed that the overtones appear also through a term that corresponds to the second term of eq 16 under such a condition.[30] This conclusion is readily understood in the framework of eq 16, by considering that the matrix element $\langle v_f|Q|v_i\rangle$ can have a nonzero value for $\Delta v > 1$ transitions when the potential minima of the i and f electronic states are displaced. With a significant potential displacement, the second term of eq 16 (the Herzberg−Teller coupling) can also give rise to the overtone in the spectra.

Obviously, the highly excited S_n state plays an essential role in the Herzberg−Teller coupling through an efficient vibronic coupling with other closely located electronic $S_{n'}$ state(s). The contribution of the vibronic coupling in the S_1 state is considered to be small because the S_1 state of *cis*-stilbene is energetically well separated from other excited states that have large optical activities. In fact, to the best of our knowledge, there have been no reports of noticeable vibronic coupling in the S_1 state of stilbene. It is also noteworthy that the resonance Raman spectra of S_0 *cis*-stilbene, which is very sensitive to the nuclear−electronic coupling in the S_1 state, was analyzed thoroughly within the Condon approximation that neglects the vibronic coupling in the S_1 state.[31] Therefore, we conclude that the 220 cm^{-1} vibration gains its signal intensity in ultrafast pump−probe as well as in resonance Raman, by the Herzberg−Teller coupling due to significant vibronic coupling in the highly excited S_n state.

Last, we mention the general implication of our conclusion. In the present study, we have shown that the totally symmetric 220 cm^{-1} vibration of S_1 *cis*-stilbene gives rise to the intense oscillation in the pump−probe experiment as well as the prominent band in resonance Raman, through the Herzberg−Teller coupling. Probably, the situation is not specific to the $S_n \leftarrow S_1$ transition of *cis*-stilbene but may be often realized also for the $S_n \leftarrow S_1$ transition of other systems, because high density of electronic excited states is expected in the higher energy region, in general. Therefore, we consider that the Herzberg−Teller coupling becomes often important when we treat the transition from the S_1 state to the highly excited S_n state. In this sense, we should be careful to apply the Condon approximation when we discuss spectroscopy of excited states such as transient absorption spectroscopy.

The significant Herzberg−Teller coupling in highly excited S_n state is not directly related to the ultrafast photoisomerization reaction of *cis*-stilbene, since the reaction takes place in the S_1 state. Nevertheless, in order to adequately interpret ultrafast pump−probe data, especially oscillatory features due to nuclear wavepacket motion, it is indispensable to understand the spectroscopic origin of the transient signal. In fact, further investigation of the nuclear wavepacket motion during ultrafast isomerization process is now in progress in our laboratory.[32]

5. Conclusion

We have investigated the visible transient absorption of the S_1 state of *cis*-stilbene, which is the precursor of ultrafast (∼1 ps) *cis*−*trans* isomerization in the excited state, by using pump−probe absorption spectroscopy with 40−50 fs time resolution. The obtained wavelength-dispersed time-resolved absorption data showed a clear ∼220 cm^{-1} oscillation that arises from a coherent nuclear motion in the S_1 state. The phase and the amplitude of the oscillation did not change across the absorption peak at 645 nm, which indicated that the oscillation appeared as the intensity modulation of the $S_n \leftarrow S_1$ absorption. To theoretically elucidate the mechanism of the observed characteristics of the oscillation, we performed a numerical simulation based on the effective linear response theory. We introduced the non-Condon effect to the effective linear response approach, and simulated the temporal spectral change of the transient absorption for the cases of the Franck−Condon coupling and the Herzberg−Teller coupling. The results of the experiment and simulation clearly indicated that the non-Condon effect is significant in the $S_n \leftarrow S_1$ transition and that the Herzberg−Teller coupling is essential for the 220 cm^{-1} motion to give rise to an oscillation in the time-resolved absorption signal. To consistently rationalize the results of the present wavelength-dispersed transient absorption experiments and the reported resonance Raman spectra of S_1 *cis*-stilbene, we concluded that the vibronic coupling of S_n state is so large that the Herzberg−Teller coupling predominantly contributes to the spectroscopic intensity of the totally symmetric 220 cm^{-1} vibration, along which the S_1 and S_0 potential minima are significantly displaced. The present work suggests the non-Condon effect can be much more often important for the electronic transition from the S_1 state to highly excited S_n states.

Acknowledgment. This paper was initially prepared for the special issue for Professor S. H. Lin. This work was supported by Grant-in-Aid for Science Research on Priority Area (No. 19056009), Grant-in-Aid for Young Scientists (B) (No. 19750019) from The Ministry of Education, Culture, Sports, Science and Technology (MEXT) and Grant-in-Aid for Scientific Research (B) (No. 19350017) from Japan Society for the Promotion of Science (JSPS).

References and Notes

(1) Ishii, K.; Takeuchi, S.; Tahara, T. *Chem. Phys. Lett.* **2004**, *398*, 400−406.
(2) Takeuchi, S.; Tahara, T. *J. Chem. Phys.* **2004**, *120*, 4768−4776.
(3) Fujiyoshi, S.; Takeuchi, S.; Tahara, T. *J. Phys. Chem. A* **2003**, *107*, 494−500.
(4) Fujiyoshi, S.; Takeuchi, S.; Tahara, T. *J. Phys. Chem. A* **2004**, *108*, 5938−5943.
(5) Matsuo, S.; Tahara, T. *Chem. Phys. Lett.* **1997**, *264*, 636−642.
(6) Lochbrunner, S.; Wurzer, A. J.; Riedle, E. *J. Chem. Phys.* **2000**, *112*, 10699−10702.
(7) Takeuchi, S.; Tahara, T. *J. Phys. Chem. A* **2005**, *109*, 10199−10207.
(8) Tahara, T.; Takeuchi, S.; Ishii, K. *J. Chin. Chem. Soc.* **2006**, *53*, 181−189.
(9) Matousek, P.; Parker, A. W.; Phillips, D.; Scholes, G. D.; Toner, W. T.; Towrie, M. *Chem. Phys. Lett.* **1997**, *278*, 56−62.
(10) Kwok, W. M.; Ma, C.; Phillips, D.; Beeby, A.; Marder, T. B.; Thomas, R. L.; Tschuschke, C.; Baranovic, G.; Matousek, P.; Towrie, M.; Parker, A. W. *J. Raman Spectrosc.* **2003**, *34*, 886−891.
(11) Baranovic, G. *J. Raman Spectrosc.* **2001**, *32*, 293−299.
(12) Fuss, W.; Kosmidis, C.; Schmid, W. E.; Trushin, S. A. *Chem. Phys. Lett.* **2004**, *385*, 423−430.
(13) Takeuchi, S.; Tahara, T. *Chem. Phys. Lett.* **2000**, *326*, 430−438.

(14) Kumar, A. T. N.; Rosca, F.; Widom, A.; Champion, P. M. *J. Chem. Phys.* **2001**, *114*, 701−724.
(15) Kumar, A. T. N.; Rosca, F.; Widom, A.; Champion, P. M. *J. Chem. Phys.* **2001**, *114*, 6795−6815.
(16) Fain, B.; Lin, S. H. *Chem. Phys. Lett.* **1993**, *207*, 287−293.
(17) Fain, B.; Lin, S. H. *Chem. Phys.* **1992**, *161*, 515−526.
(18) Fain, B.; Lin, S. H.; Khidekel, V. *Phys. Rev. A* **1993**, *47*, 3222−3239.
(19) Pollard, W. T.; Dexheimer, S. L.; Wang, Q.; Peteanu, L. A.; Shank, C. V.; Mathies, R. A. *J. Phys. Chem.* **1992**, *96*, 6147−6158.
(20) Pollard, W. T.; Mathies, R. A. *Annu. Rev. Phys. Chem.* **1992**, *43*, 497−523.
(21) Taneichi, T.; Fuji, T.; Yuasa, Y.; Kobayashi, T. *Chem. Phys. Lett.* **2004**, *394*, 377−382.
(22) Rosca, F.; Ionascu, D.; Kumar, A. T. N.; Demidov, A. A.; Champion, P. M. *Chem. Phys. Lett.* **2001**, *337*, 107−116.
(23) Mukamel, S. *Principles of Nonlinear Optical Spectroscopy*; Oxford University Press: New York, 1995.
(24) Tanimura, Y.; Mukamel, S. *J. Opt. Soc. Am. B* **1993**, *10*, 2263−2268.
(25) Khidekel, V.; Chernyak, V.; Mukamel, S. *J. Chem. Phys.* **1996**, *105*, 8543−8555.
(26) Fragnito, H. L.; Bigot, J.-Y.; Becker, P. C.; Shank, C. V. *Chem. Phys. Lett.* **1989**, *160*, 101−104.
(27) Ernsting, N. P.; Kovalenko, S. A.; Senyushkina, T.; Saam, J.; Farztdinov, V. *J. Phys. Chem. A* **2001**, *105*, 3443−3453.
(28) Rubtsov, I. V.; Yoshihara, K. *J. Phys. Chem. A* **1999**, *103*, 10202−10212.
(29) Kano, H.; Saito, T.; Kobayashi, T. *J. Phys. Chem. A* **2002**, *106*, 3445−3453.
(30) Albrecht, A. C.; Clark, R. J. H.; Oprescu, D.; Owens, S. J. R.; Svendsen, C. *J. Chem. Phys.* **1994**, *101*, 1890−1903.
(31) Myers, A. B.; Mathies, R. A. *J. Chem. Phys.* **1984**, *81*, 1552−1558.
(32) Takeuchi, S.; Ruhman, S.; Tahara, T. Manuscript in preparation.